Arch. Metall. Mater. **63** (2018), 1, 387-391

DOI: 10.24425/118952

L. WANG*#, X. WANG**, G. ZHANG*, X. SUN*

PHASE TRANSITION AND PLASTICITY ENHANCEMENT OF Ti-Cu-BASED BULK METALLIC GLASSES

In this paper, we report the complex crystallization kinetics of phase transition happening in Ti-Cu-based bulk metallic glasses (BMGs), which play significant roles in the glass formation with respect to their low reduced glass transition temperatures, T_{rg}. The first exothermic event just occurs when annealing the BMG samples in the supercooled liquid region, leading to the Avrami exponent deviating from conventional modes affected by the residual amorphous phase. For $Ti_{43}Cu_{43}Ni_7Zr_7$ BMG, the plasticity can be improved by pre-annealing at a sub-T_g temperature of 623K (≈50K below T_g) for 0.5 hour, however, deteriorated by 1 hour annealing, which could be related to the change in stability of this BMG against crystallization with different pre-annealing times.

Keywords: Bulk metallic glasses; Phase transition; Annealing; Stability; Plasticity

1. Introduction

Bulk metallic glasses (BMGs) using common metals (Cu, Ti, Ni, Fe, etc.) as the major component have been drawing much attention for their low cost and superior properties [1-5]. So far, the critical size of common-metal-based BMGs by copper mold casting can be over 5 mm or even more. For example, with minor Y addition, the maximum size of Fe-based or Cu-based BMGs can reach 10 mm in diameter [5,6]. Also, Ti-based BMGs, usually being regarded as potential biomaterials, can be cast into 8 mm amorphous rods in diameter with Be addition [7]. However, rare earth (Er, Y) or toxic metal (Be) addition, in some sense, is a serious restriction for their industrial applications. In fact, when only using common metals under suitable rules of alloying design, high glass-forming ability can be achieved. One of them is the equiatomic substitution, such as the composition examples of $(Cu_{50}Zr_{50})_{100-x}Al_x$ (x = 4 to 8 at.%) [8] and $Cu_{43}Zr_{43}Ag_7Al_7$[9]. Note that the binary composition point of 50/50 is special, which provides a favorable initial start for the amorphous phase to generate. Then the substitution of Cu/Zr by other elements requires in equiatomic content simultaneously to increase the topological packing without extra strong interactions appearing between atoms of any two elements. More interestingly, it is found that this rule is also effective in $Ti_{50}Cu_{50}$ system. To understand the stability and glass forming ability of Ti-Cu-based BMGs, crystallization behaviors are studied upon heating to reveal the kinetic process of crystalline phases precipitated from the amorphous matrix.

In addition, the brittleness of BMGs has been exposed seriously, becoming a great challenge for their practical applications [10]. Usually, the structural relaxation in BMGs happens upon heating or isothermal annealing before the onset of crystallization, being considered as a process for BMGs to lose their ductility [11,12]. Recently, the four R's tactics have been proposed to improve the tensile ductility of MGs at room temperature [13]. In contrast, for a Ti-Cu-based BMG, the ductility is not decreased but increased at the beginning of a sub-T_g annealing, and the possible reason for this phenomenon is also discussed.

2. Experimental methods

Pre-alloyed ingots of nominal compositions listed in Table 1 were prepared by arc melting technique under a Ti-gettered purified Argon atmosphere. High-purity elements of Ti, Cu, Zr, Ni, and Sn with purities higher than 99.9% were used as raw materials. Each alloy ingot of about 3 g was remelted several times to improve the homogeneity, and then sucked into a water-cooled copper mold. The rods in 1, 2 and 3 mm diameter were cast, respectively. Structural analyses were conducted using an x-ray diffractometer (Philips X'Pert) with Cu-Ka radiation. A differential scanning calorimetry (Perkin-Elmer diamond DSC) was utilized to investigate the isochronal and isothermal crystallization kinetics under the Argon atmosphere. A differential thermal analyzer (DTA S-1600) was adopted to detect the melting point and liquidus temperature of each alloy. Cylindrical specimens of 2 mm diameter and 4 mm length were prepared from as-cast rods, and both ends were polished to make them parallel to each other. The compressive mechanical tests were performed on an Instron machine using a strain rate of 10^{-4} s^{-1}

* SCHOOL OF MECHANICAL AND ELECTRICAL ENGINEERING, CHIZHOU UNIVERSITY, CHIZHOU 247000, CHINA
** SCHOOL OF MATERIALS SCIENCE AND ENGINEERING, ZHEJIANG UNIVERSITY, HANGZHOU 310027, CHINA
# Corresponding author: lielongwang@126.com

TABLE 1

Characteristic temperatures detected by DTA scans, supercooled liquid region ($\Delta T_x = T_x - T_g$), reduced glass transition temperature ($T_{rg} = T_g/T_l$), and a parameter of glass-forming ability ($\gamma = T_x/(T_g + T_l)$) as well as Vicker's hardness H_v (kg/mm^2) of Ti-Cu-based BMGs

Alloys	T_g (K)	T_x (K)	T_m (K)	T_l (K)	ΔT_x	T_{rg}	γ	H_v
(a) $Ti_{41}Cu_{41}Ni_9Zr_9$	680	703	1090	1199	23	0.57	0.358	588
(b) $Ti_{43}Cu_{43}Ni_7Zr_7$	678	701	1114	1212	23	0.56	0.354	567
(c) $Ti_{43}Cu_{40.5}Ni_7Zr_7Sn_{2.5}$	693	718	1118	1212	25	0.57	0.359	592
(d) $Ti_{45}Cu_{40}Ni_{7.5}Zr_5Sn_{2.5}$	690	720	1140	1207	30	0.57	0.358	596

at room temperature. Fractography and shear bands on the specimen surface were observed by using a scanning electron microscope (SEM).

3. Results and discussion

BMGs are thermodynamically metastable and would transform into stable phase upon heating. Fig. 1 shows the glass transition, crystallization and following melting process of each BMG by a DTA scan at a heating rate of 20 K/min. The characteristic temperatures are listed in Table 1, from which one can see that the glass transition temperature T_g and the onset temperature of crystallization T_x are increased by minor Sn substitution. However, the glass-forming ability of these Ti-Cu-based BMGs measured by the parameter of T_{rg} is quite low (<0.60), similar to the report of $Ti_{34}Zr_{11}Cu_{47}Ni_8$ alloy whose T_{rg} value is of about 0.578 [14]. The critical size in diameter of BMGs from (a) to (d) by Cu mold casting is about 3 mm, and only 4 mm in the fully amorphous state for alloy (b) $Ti_{43}Cu_{43}Ni_7Zr_7$ with the lowest T_{rg} value instead. Also, Fig. 1 displays multiple-step transformations of crystallization for each alloy, and Sn addition reducing the number of exothermic events from 4 to 3. To understand the phase transition in detail during crystallization, several stops were made by the end of each exothermic event upon DSC scanning and then the samples were detected by x-ray diffraction(XRD). Fig. 2 shows XRD patterns of the as-cast alloy (b) $Ti_{43}Cu_{43}Ni_7Zr_7$ and (d) $Ti_{45}Cu_{40}Ni_{7.5}Zr_5Sn_{2.5}$, and also the phase precipitation after each exothermic event, respectively. The results show that XRD patterns of as-cast alloys exhibits a broad diffraction peak, typically for the glassy structure, and that there are four exothermic events of crystallization in the alloy (b) appearing in the following route: Am → Am' → unknown phase → Laves phase → γ-TiCu, however, in the alloy (d) three events of crystallization proceed along the course of Am → bcc β-Ti → unknown phase → γ-TiCu. It was reported [15] that the Laves phase with $MgZn_2$-type structure appears in the Ti-Zr-Ni system usually as final stable phase. However, the Laves phase detected in the alloy (b) is just as a transitional phase with lattice constant of about $a = 0.502$ nm and $c = 0.819$ nm, and the final stable phase is γ-TiCu.

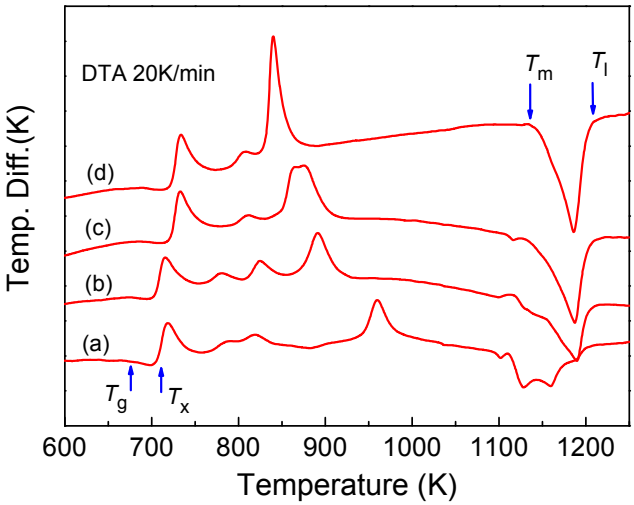

Fig. 1. DTA scans for the alloys from (a) to (d) listed in Table 1 at a heating rate of 20 K/min

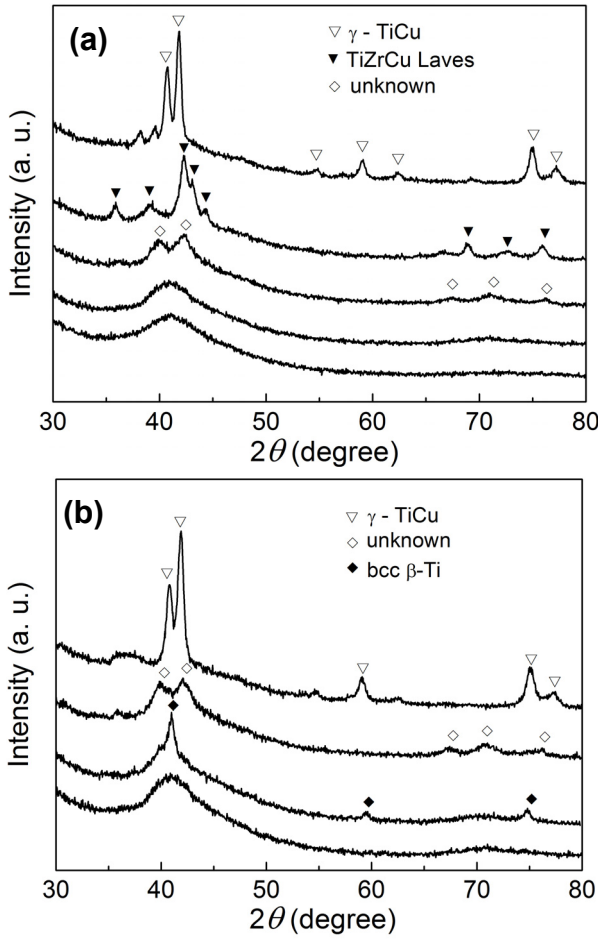

Fig. 2. (a) XRD patterns for the phase precipitation happening after each exothermic event in the $Ti_{43}Cu_{43}Ni_7Zr_7$ alloy and (b) in the $Ti_{45}Cu_{40}Ni_{7.5}Zr_5Sn_{2.5}$ alloy, respectively

In order to calculate the activation energy of each phase to precipitate in the alloy (b) and alloy (d), the isochronal heating mode was exploited by using DSC at different heating rates of 5, 10, 20 and 40K/min, respectively. Then the activation energy for crystallization can be evaluated by using Kissinger's equation [16]:

$$\ln(\beta/T_p^2) = -E_a/RT_p + C \quad (1)$$

where β is the heating rate, T_p is the peak temperature, and R is the gas constant. A straight line was obtained by fitting the relationship between $\ln(\beta/T_p^2)$ and $1/T_p$. The activation energy calculated for the crystallization of each phase was displayed in Fig. 3. It is obvious that from the amorphous phase to the γ-TiCu in the alloy (b) needs to pass through four-step transformations and the first three steps have rather high activation energy of 331.8, 309.1 and 368.9 kJ/mol, respectively. However, only three-step transformations happen in the alloy (d) from the amorphous phase to the γ-TiCu, and the activation energy is quite low about 293.3 kJ/mol for the primary phase of the bcc β-Ti to precipitate. Usually, the high glass forming ability (GFA) depends on the competition between the metastable crystalline phases and the amorphous phase. Therefore, although the magnitude of parameter T_{rg} of these two BMGs is low and nearly the same, the complicated crystallization kinetics and sluggish atomic movement are really dominant factors to restrain the formation of crystalline phases, accordingly leading to the higher GFA of the alloy (b) than the alloy (d).

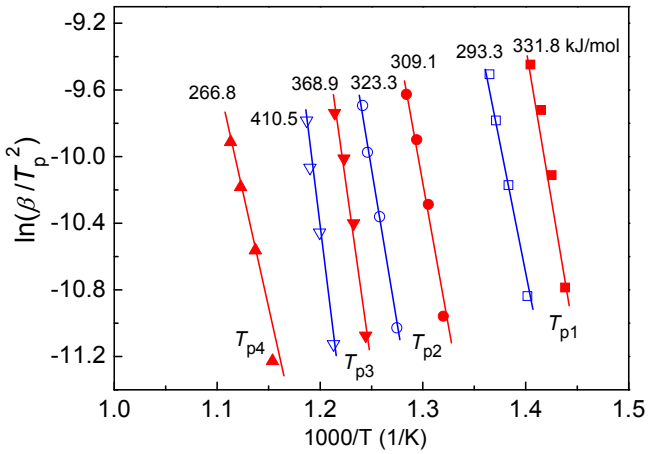

Fig. 3. Activation energy obtained by Kissinger' equation using the T_p temperature for each phase transition of $Ti_{43}Cu_{43}Ni_7Zr_7$ (solid) and $Ti_{45}Cu_{40}Ni_{7.5}Zr_5Sn_{2.5}$ (open) alloys

Isothermal annealing has also been conducted to investigate the crystallization behaviors of the alloy (b) and alloy (d). The sample was heated to the temperature of 693K at a rate of 100K/min for avoiding the structural relaxation, and then holding the temperature until an exothermic event was completed. The volume of the crystalline phase (x_v) at time t was obtained based on the fractional area of the exothermic event with respect to the whole. Because the T_x temperature of alloy (d) is higher than that of alloy (b), the time of isothermal crystallization for the alloy (d) is of about 18 min and for the alloy (b) only about 5 min. The isothermal crystallization kinetics of amorphous alloys is normally analyzed using the Johnson-Mehl-Avrami (JMA) equation [17]:

$$n(x) = \frac{\partial \ln[-\ln(1-x_v)]}{\partial \ln(t-t_0)} \quad (2)$$

where t_0 is the incubation time, and n is the so-called Avrami exponent, which can be used to characterize the nucleation and growth mode of precipitates during isothermal annealing, being 3.0 for a constant number of quenched-in nuclei and 4.0 for a constant nucleation rate. Fig. 4 (a) shows the Avrami exponents of these two alloys changing with increase of volume fraction of crystallites obtained by equation (2). Unlike the conventional JMA mode that Avrami exponent basically keeps a constant, Avrami exponents of alloy (b) and (d) are lower than 3.0, decreasing in the middle stage of transformation and then showing an abnormal rise at high x_v, indicating that they may be controlled by the similar crystallization mode. Comparing DSC scans of the isothermal annealed samples with the as-cast alloy (b) and (d) as shown in Fig. 4 (b), it is evident that there is just the first

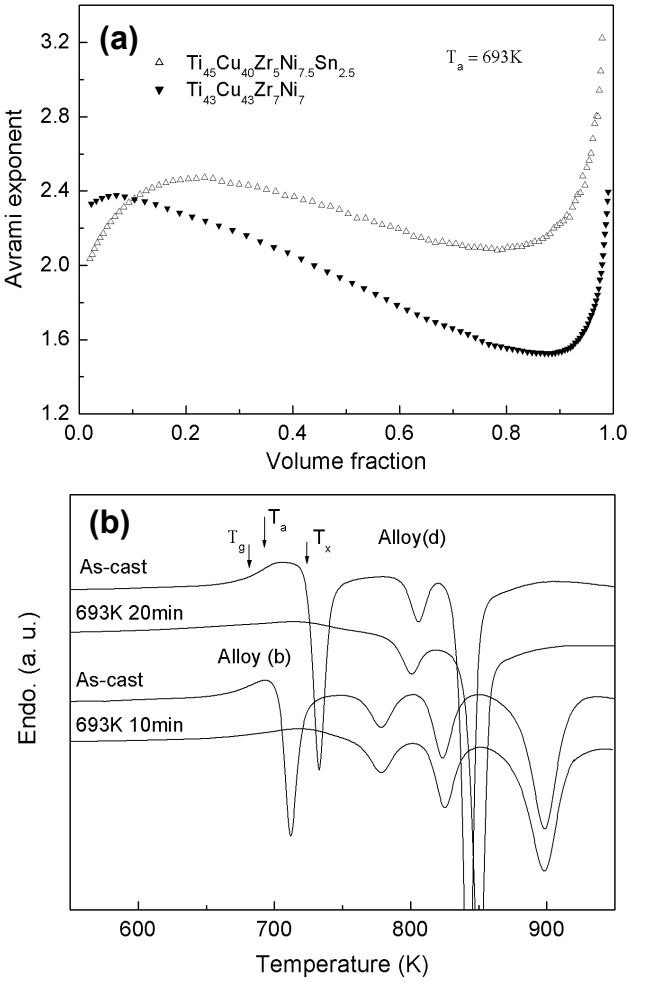

Fig. 4. (a) Avrami exponents of alloy (b) and (d) changing with volume fraction of crystallites upon 693K isothermal annealing, and (b) DSC scans of isothermal annealed samples of alloy (b) and alloy (d) compared with as-cast samples

exothermic event happening during the isothermal annealing. Kelton [18] confirmed that the equation (2) is not valid for polymorphic transformation when the nucleation barrier is large. And the similar phenomenon was observed during the isothermal annealing for a $Zr_{57}Cu_{20}Al_{10}Ni_8Ti_5$ [19] amorphous alloy with multiple-step crystallization behavior. They proposed that the increasing crystallization temperature of residual amorphous phase might affect the crystal nucleation rate and the growth rate, such as heterogeneous nucleation [20] and diffusion-controlled anisotropic growth [21] and be responsible for this anomalous Avrami exponent. However, it seems that the isothermal annealing of Ti-Cu-based BMGs in the supercooled liquid region is a preferable way to prepare the amorphous matrix composites reinforced by the nano-sized primary phases.

Experiments have indicated that metallic glasses tested in the uniaxial tension show nearly zero plastic strain prior to the failure, however, overall 0 ~ 2% plastic strain is usually observed in the uniaxial compression [22, 23]. Plastic deformation is ascribed to the accumulation of shear bands, which initiate and rapidly propagate across the sample at the angle of approximately 45° to the loading axis. It is assumed that the vein pattern on the fracture surfaces of BMGs is due to the meniscus instability caused by local adiabatic deformation heating [24]. A rapid increase in the temperature of the material inside the catastrophic shear bands makes the local materials soften and rupture. Usually, low temperature ($<T_g$) annealing can cause BMGs to lose their ductility and become brittle, such as a report for La-based BMGs [12]. However, in our uniaxial compression test, the plastic strain for an as-cast $Ti_{43}Cu_{43}Zr_7Ni_7$ BMG is of about 3%, whereas increases to 6% for a 623K-0.5hr-annealed sample, and decreases to 1% for a 623K-1hr-annealed sample. Fig. 5 shows the distribution of shear bands on the specimen surface after fracture. Very limited shear bands are observed on the specimen surface of the as-cast $Ti_{43}Cu_{43}Zr_7Ni_7$ BMG. However, many shear bands are obviously increased and accumulated on the surface of 0.5 hr-annealed samples for their improved plasticity, and almost no shear bands appear on the 1hr-annealed samples due to its increased brittleness. XRD patterns show that all these samples are still in the fully amorphous structure and no crystalline phases are detected. However, the DSC scans as illustrated in Fig. 6 show that the exothermic events happening in the 623K-0.5hr-annealed sample shift to the high temperatures of about 5 K and the enthalpy increases about 5 J/g for the last event (Laves phase → γ-TiCu) in comparison with the as-cast one, suggesting that 0.5hr pre-annealing at 623K makes this Ti-Cu-based BMG more stable against following crystallization. With extension of annealing time to 1 hour, the peaks gradually approach to the positions of the as-cast sample. As such, 623K-0.5hr-annealing for the $Ti_{43}Cu_{43}Zr_7Ni_7$ BMG, not only improves its plasticity but also its strength. Usually, the sub-T_g annealing is proved to promote the formation of critical clusters and cause the following crystallization more easily to happen. However, in this case, structural relaxation in the $Ti_{43}Cu_{43}Zr_7Ni_7$ BMG induced by 623K-0.5hr-annealing maybe makes the material more disorder and homogeneous, or promotes the formation of ordering clusters very different from the structure of the primary phase so that it becomes more difficult for the following crystallization to happen. Therefore, the enhanced plasticity of $Ti_{43}Cu_{43}Zr_7Ni_7$ BMG may be due to the increased stability against crystallization after 623K-0.5hr-annealing, as indicated in some refs. [25,26].

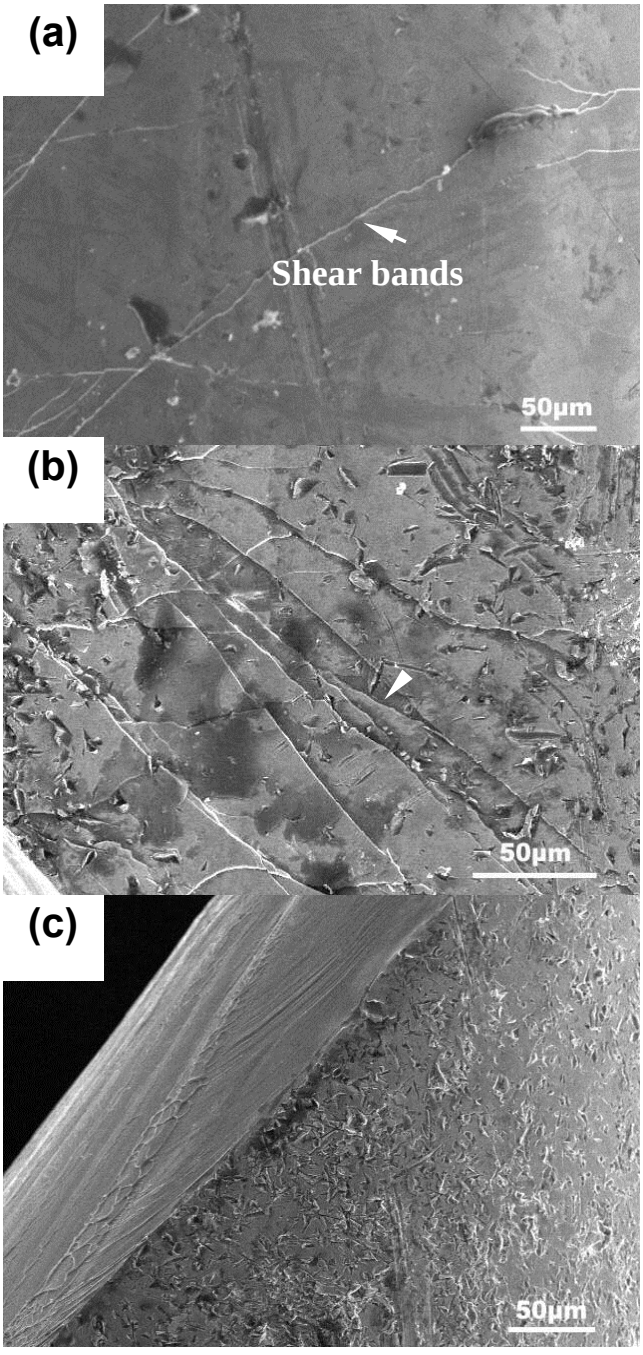

Fig. 5. The morphology of shear bands on the specimen surface of (a) as-cast (b) 623K-0.5hr-annealed and (c) 623K-1hr-annealed samples of $Ti_{43}Cu_{43}Ni_7Zr_7$ alloy after fracture under uniaxial compression

It was reported [27,28] that nanocrystallization could be triggered by deformation in and around the shear bands during indentation or compression tests, which can act as barriers to prevent the propagation of shear bands. On the other hand, they can also initiate cracks to make BMGs rupture for stress

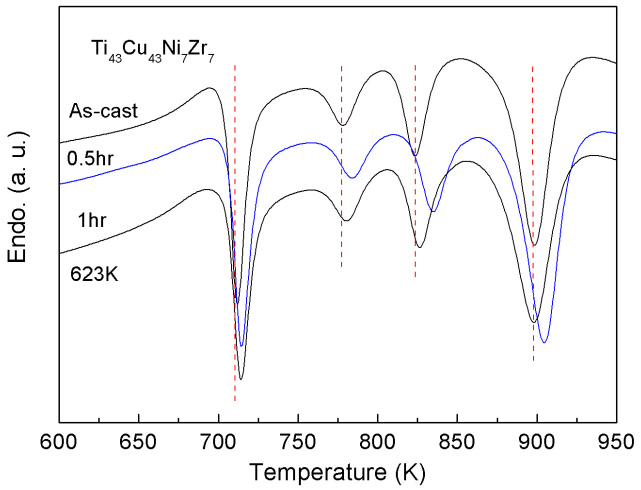

Fig. 6. DSC scans of as-cast and 623K-0.5hr and 1hr-preannealed samples of $Ti_{43}Cu_{43}Ni_7Zr_7$ BMG, respectively

concentration. Thus, when monolithic BMGs had homogeneous structure or stable short-range ordering, as well as sluggish atomic diffusion against nanocrystallization during deformation, the good plasticity could be achieved. From this point of view, the stability of BMGs should also have some close relationship with their plasticity enhancement.

4. Conclusions

Without noble metal and rare-earth metal addition, equiatomic substitution of Ti and Cu with Zr, Ni and Sn makes Ti-Cu-based BMGs present the strong glass forming ability and complex crystallization behavior. A series of phase transitions happen prior to precipitation of the final stable phase of γ-TiCu. Upon isothermal annealing, there is only the first exothermic event happens whose crystallization behavior does not obey the conventional JMA equation affected by the residual amorphous phase. For the $Ti_{43}Cu_{43}Zr_7Ni_7$ BMG, pre-annealing at 623K for 0.5 hour does not make the BMG brittle but improve its plasticity, which may be related to the increased stability by 623K-0.5hr annealing.

Acknowledgements

This study was financially supported by National Natural Science Foundation of China (No. 51005026).

REFERENCES

[1] H.B. Lou, X.D. Wang, F. Xu et al., Appl. Phys. Lett. 99, 051910 (2011).
[2] H. Men, S.J. Pang, A. Inoue, T. Zhang, Mater. Trans. **46**, 2218 (2005).
[3] M.Q. Tang, H.F. Zhang, Z.W. Zhu et al., J. Mater. Sci. Technol. **26**, 481 (2010).
[4] J.H. Na et al., Proc. Natl. Acad. Sci. USA **111**, 9031 (2014).
[5] Z.P. Lu, C.T. Liu, J.R. Thompson, W.D. Porter, Phys. Rev. Lett. **92**, 245503 (2004).
[6] D.H. Xu, G. Duan, W.L. Johnson, Phys. Rev. Lett. **92**, 245504 (2004).
[7] Y.C. Kim, W.T. Kim, D.H. Kim, Mater. Sci. Eng. A **375**, 127-135 (2004) .
[8] P. Yu, H.Y. Bai, M.B. Tang, W.L. Wang, J. Non-Cryst. Solids **351**, 1328 (2005).
[9] D.S. Sung, O. Kwon, E. Fleury, K.B. Kim, J.C. Lee, D.H. Kim, Y.C. Kim, Metals and Mater. Inter. **10**, 575 (2004).
[10] A.L. Greer, Y.Q. Cheng, E. Ma, Mater. Sci. Eng. R **74**, 71 (2013).
[11] P. Murali, R. Ramamurty, Acta Mater. **53**, 1467 (2005).
[12] U. Ramamurty, M.L. Lee, J. Basu, Y. Li, Scripta Mater. 47, 107 (2002).
[13] E. Ma, J. Ding, Ma, E., and J. Ding, Materials Today (2016).
[14] X.H. Lin, W.L. Johnson, J. Appl. Phys. **78**, 6514 (1995).
[15] J.B. Qiang, Y.M. Wang, D.H. Wang, M. Kramer, C. Dong, Philos. Mag. Lett. **83**, 467 (2003).
[16] H.E. Kissinger, Anal. Chem. **29**, 1702 (1957).
[17] A. Calka, A.P. Radlinski, J. Mater. Res. **3**, 59 (1987).
[18] K.F. Kelton, J. Non-Cryst. Solids **163**, 283 (1993).
[19] L.Q. Xing, J. Eckert, W. Löser, L. Schultz, D.M. Herlach, Philos. Mag. A **79**, 1095 (1999).
[20] N.X. Sun, X.D. Liu, K. Lu, Scripta Mater. **34**, 1201 (1995).
[21] A.S. Bakai, H. Hermann, N. P. Lazarev, Philos. Mag. A **82**, 1521 (2002).
[22] H.A. Bruck, T. Christman, A.J. Rosakis, W.L. Johnson, Script Metall. Mater. **30**, 429 (1994).
[23] L.Q. Xing, C. Bertrand, J.-P. Dallas, M. Cornet, Mater. Sci. Eng. **A241**, 216 (1998).
[24] A.S. Argon, M. Salama, Mater. Sci. Eng. **23**, 219 (1976).
[25] X.D. Wang, L. Yang, J.Z. Jiang, K. Saksl, H. Franz, H.-J. Fecht, Y.G. Liu , H.S. Xian, J. Mater. Res. **22**, 2454 (2007).
[26] M.W. Chen, A. Inoue, W. Zhang, T. Sakurai, Phys. Rev. Lett. **96**, 245502 (2006).
[27] J.J. Kim, Y. Choi, S. Suresh, A.S. Argon, Science **295**, 654 (2002).
[28] D.T.A. Matthews, V. Ocelik, P.M. Bronsveld, J.Th.M. De Hosson, Acta. Mater. **56**, 1762 (2008).